THE JOURNAL OF PHYSICAL CHEMISTRY C

Article

pubs.acs.org/JPCC

Molecular Dynamics Simulation of the Adsorption and Aggregation of Ionic Surfactants at Liquid−Solid Interfaces

Felipe Jiménez-Ángeles,[†] Atefeh Khoshnood,[†] and Abbas Firoozabadi*[,†,‡]

[†]Reservoir Engineering Research Institute, Palo Alto, California 94301, United States

[‡]Department of Chemical and Environmental Engineering, Yale University, New Haven, Connecticut 06510, United States

Supporting Information

ABSTRACT: Structure of surfactants adsorbed on solid surfaces is a key knowledge in various technologies and applications. It is widely accepted in the literature that the surface−surfactant headgroup electrostatic interaction is a major driving force of adsorption of ionic surfactants on charged substrates. Our result shows that the adsorption of surfactants as monomers is driven by both electrostatic and nonelectrostatic interactions. Further adsorption of surfactants in aggregates is essentially driven by the tail−tail interaction. To a great extent, the substrate−tail interaction determines the structures of the adsorbed surfactant aggregates. Water and counterions influence the headgroup−substrate and tail−substrate interactions. We investigate two vastly different surfactants and substrates by molecular dynamics simulations: (1) SDS on alumina (SDS−Al_2O_3), and (2) CTAB on silica (CTAB−SiO_2). We study the adsorption of a single surfactant at the solid surface by the density profiles and free energy of adsorption. In the SDS−Al_2O_3 system, we analyze the free energy of adsorption on the substrate covered by aggregates of different sizes. We examine the configurations of surfactants and the distribution of water and ions at the liquid−solid interface as the number of adsorbed molecules on the substrate increases. In the SDS−Al_2O_3 system, the headgroup adsorption is mediated by the Na^+ counterions; the adsorbed water molecules may be displaced by the surfactant headgroup but unlikely by the hydrocarbon tails. As a function of the surfactant adsorption, we observe single surfactants, aggregates of different morphologies, and bilayers. The CTAB−SiO_2 system combines both electrostatic attraction of the surfactant headgroup and affinity for the surfactant's hydrocarbon tail. At low surfactant adsorption, aggregates and single surfactant molecules lie on the substrate; hemimicelles form at intermediate adsorption; and micelles form at high surfactant adsorption. Our results agree with experimental observations and indicate two different surfactant adsorption mechanisms where the tail−tail and tail−substrate interactions play a fundamental role.

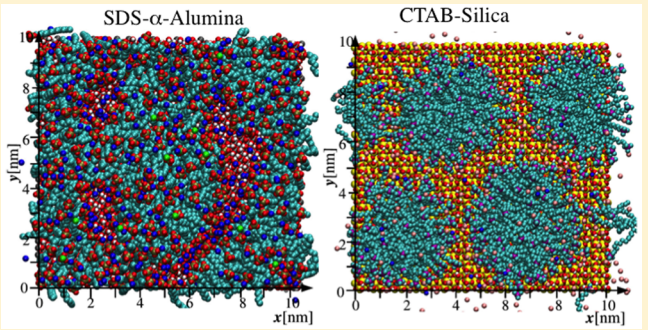

INTRODUCTION

Surfactants are functional molecules consisting of a hydrocarbon tail and a headgroup (ionic or nonionic).[1] Adsorption of surfactants on surfaces from aqueous solutions is the basis of a variety of technological applications such as froth flotation,[2] enhanced oil recovery,[3] biotechnological processes,[4,5] pollutant removal from environment,[6,7] among many others. The morphology of the aggregates adsorbed on surfaces is determined by the ionic or nonionic character of the headgroup, the surface charge of the substrate, the strength of interactions between chains, the hydrophobicity and hydrophilicity of the surface, the ionic concentration in the solution, and pH. The adsorption of nonionic surfactants with a poly(ethylene oxide) $(EO)_n$ headgroup on silicon dioxide is an example where the electrostatic attraction between surfactant and the surface is weak.[8−11] The measurements indicate that a short surfactant headgroup $(EO)_6$ forms bilayers,[8−10] whereas a long surfactant headgroup $(EO)_{25}$ forms spherical aggregates.[8] Stable monolayers are observed in the adsorption of carboxylated surfactants on fluorite[12−14] when there is electrostatic attraction between the surface and the surfactant headgroup.

The adsorption of a surfactant on a solid substrate is determined by measuring the residual surfactant concentration in bulk.[8,15] Usually the adsorption isotherms are reported as the number of molecules per surface area as a function of the residual (equilibrium) bulk concentration. In a variety of systems the adsorption isotherms assume two general shapes referred to as the four-region isotherm[15−17] and the two-step isotherm[18−20] (see Figure S1 in the SI). A correlation between the isotherm shape and the morphology of the aggregates is suggested. The two-step adsorption isotherm is usually plotted in a linear scale and consists of two steps (see Figure S1a in the SI). In step 1 (s-1) the surfactants are adsorbed as individual molecules through interactions with the surface. In the second step (s-2), the adsorbed surfactants form "surface micelles" until the surface is saturated.[17] The two-step isotherm is observed in different surfactants adsorbed on silica.[18−23] In the

Received: September 24, 2017
Revised: October 23, 2017
Published: October 24, 2017

DOI: 10.1021/acs.jpcc.7b09466
J. Phys. Chem. C XXXX, XXX, XXX−XXX

adsorption isotherm of some ionic surfactants on hydrophilic surfaces, three slope changes and a plateau in a log−log scale define four regions (see Figure S1b in the SI).[15−17] The individual surfactants adsorb electrostatically in region I. In region II the surfactants associate as hemimicelles with the headgroups oriented toward the solid surface, and the hydrocarbon tails are in contact with the aqueous phase. Higher concentration increases the number of surfactant aggregates, and some molecules adsorb with opposite orientation. In region III the adsorption is through the growth of aggregates formed in stage II turning into bilayers. In region IV a bilayer is completely formed, and the surface does not adsorb more surfactants.[17] Ionic surfactants adsorbed on alumina, silica gel, rutile, and cellulose follow the four-region trend.[24]

Linear and nonlinear spectroscopic techniques,[25] neutron reflectometry,[26−28] small-angle neutron scattering,[29] and atomic force microscopy[30] are used to investigate the morphology of the surfactant aggregates adsorbed on substrates. A variety of structures have been deduced for different surfactants and substrates. Using sum-frequency spectroscopy and Raman scattering, centrosymmetric aggregates have been resolved for cetyltrimethylammonium bromide (CTAB) adsorbed on amorphous silica.[25] Two headgroup orientations, one pointing toward the substrate and one pointing toward the solution phase, are suggested from spectroscopic measurements of sodium dodecyl sulfate (SDS) adsorbed onto positively charged films.[31] Atomic force microscopy experiments reveal hemimicelles and hemicylindrical structures of ionic surfactants on hydrophobic substrates.[32−34]

Coarse grain and atomistic molecular dynamics simulations are employed to study the aggregation morphologies of surfactants adsorbed on different solid surfaces.[35−44] A variety of morphologies are observed in MD simulations of SDS adsorbed on a silica surface with different degrees of hydroxylation and charge density.[36,41] Bilayers have been observed in MD simulations of sodium sulfate surfactants (with single and double tail) adsorbed on alumina.[37] Surfactant adsorption and water structure have been investigated in surfaces such as graphite and carbon nanotubes.[38,44,45] Previous studies have not addressed the adsorption of single surfactants on mineral substrates. Basic questions related to the interaction of a single surfactant with a surface and how it is related to the morphology of the aggregates remain open.

In this work, we perform MD simulations to investigate the free energy of adsorption of single surfactants on a solid surface. Then we analyze the morphology of the aggregates by varying the number of surfactants adsorbed on the substrate. We choose two systems widely investigated experimentally: (1) SDS on α-alumina (SDS−Al_2O_3) and (2) CTAB on silica (CTAB−SiO_2). The first represents a system exhibiting a four-region isotherm, while the second shows a two-step isotherm. We observe significant differences between the two systems related fundamentally to the way the surfactant tail is adsorbed on the surface. Even the adsorption of a single surfactant molecule is significantly different in the two systems. Our first objective is to determine the interaction of surfactants and mineral substrates using MD simulations. Second we characterize the morphology of aggregates formed by the adsorbed surfactants. Finally, we shed light on the adsorption mechanisms. The paper is organized in three sections. First, we present the models and simulation methods. Second, the results are split in a subsection for SDS adsorption on α-alumina and a subsection for CTAB adsorption on silica. Finally conclusions are drawn.

METHODS

We investigate the adsorption of surfactants on a mineral substrate. The molecular structure of the surfactants sodium dodecyl sulfate (SDS) and cetyltrimethylammonium bromide (CTAB) and the mineral substrates α-alumina (α-Al_2O_3) and silica α-cristobalite (SiO_2) are shown in Figure 1a. The alumina substrate is built by cleavaging the α-Al_2O_3 crystal[46] along the oxygen-terminated (0001) surface which is then fully protonated to give rise to a hydroxyl-terminated surface. The hydrogen atoms are bonded to oxygen atoms of the alumina, but they are free to rotate around the oxygen atoms. Fully hydroxyl-terminated surfaces yield an OH coverage of 15.5 per nm^2. According to ab initio simulations, a fully protonated surface of α-alumina is favored in the presence of water.[47] The total charge of the solid is zero. The thickness of the alumina slab from the center of aluminum atoms at the bottom to the center of oxygen atoms at the top is 1.2 nm. The z coordinate of the center of oxygen atoms in the hydroxyl group of alumina is defined as $z = 0$. The silica substrate is built by cleavaging the

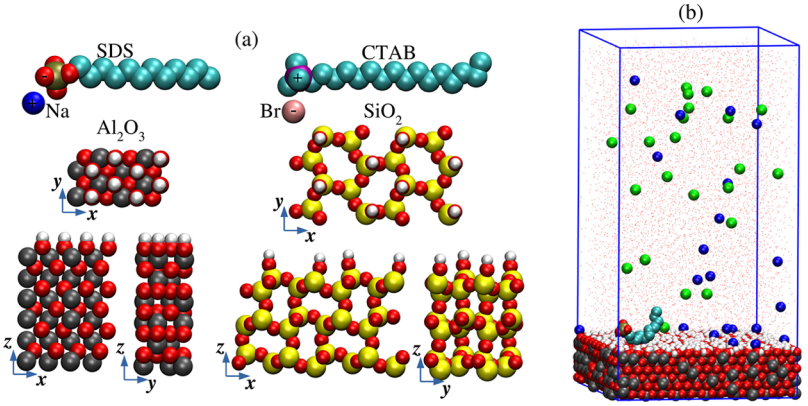

Figure 1. (a) Sodium dodecyl sulfate (SDS) and cetyltrimethylammonium bromide (CTAB) and crystalline structures of α-alumina (Al_2O_3) and silica α-cristobalite (SiO_2), simply referred to as silica. (b) Snapshot of a simulation box containing NaCl aqueous solution and a single SDS molecule adsorbed on the alumina surface. The snapshot is for Run 1A in Table S1. The composition and box sizes of the simulated systems are given in Tables S1 and S2. The color code is as follows: Sodium (Na^+) is dark blue, chlorine (Cl^-) is green, bromide (Br^-) is pink, sulfur (S) is tan, nitrogen (N) is purple, aluminum is gray, silicon is yellow, oxygen is red, hydrogen is white, and methyl (CH_3) and methylene (CH_2) groups are cyan.

DOI: 10.1021/acs.jpcc.7b09466
J. Phys. Chem. C XXXX, XXX, XXX−XXX

silica α-cristobalita crystal on the 101 plane. Hereinafter silica α-cristobalite is simply referred to as silica. The exposed silanol groups are at a surface density of 4.7 per nm^2. A full protonation of silanol groups results in a hydroxyl-terminated surface and occurs at pH = 2. In our simulations we assume pH = 7 where about 9% of the silanol groups of silica are not protonated which translates into a surface charge density of 0.43 O^- atoms/nm^2 (−6.9 μC/cm^2) on the surface of silica.[48−50] The charge of silica is balanced by Na^+ ions in the solution; 11 Na^+ ions are required to balance the charge of a silica surface of about 5.2 × 4.9 nm^2. Hydrogen atoms are free to rotate around the oxygen atoms of silica. The thickness of a silica slab from the center of aluminum atoms at the bottom to the center of oxygen atoms at the top is about 2.2 nm. The SPC/E model[51] is employed for water and the OPLS united atom model[52] for the surfactants' tail. The parameters in refs 37 and 53 are used for the sulfate and trimethylammonium headgroups, respectively. Alumina is modeled using the CLAYFF parameters,[54] while silica is represented using the parameters from ref 50. The charge of each atom or group in alumina and the surfactant molecule is presented in Table S3.

Our systems consist of a slab of the mineral substrate next to an aqueous solution containing the surfactant molecules. The simulation box is prismatic with the size of $L_x \times L_y \times L_z$ along the x, y, and z directions, respectively. The z-direction is perpendicular to the solid surface exposed to aqueous solution. Periodic boundary conditions are imposed in the x- and y-directions. In the z-direction the simulation box is constrained by a virtual wall imposed by means of a 9-3 Lennard-Jones potential: $u_{ij}^{w}(z) = 4\epsilon_w \pi \rho_w \sigma_w^3/3\ [(\sigma_w/z)^9/15 - (\sigma_w/z)^3/2]$; ρ_w = 20 atoms/nm^3, ϵ_w = 1.3 kJ/mol, and σ_w = 0.37 nm.[55] The box length in the z-direction is adjusted to keep the average pressure around 100 bar.

We employ different box sizes in our simulations. A snapshot of the simulated box employed to calculate the potential of mean force and to simulate the adsorption of a single surfactant molecule is shown in Figure 1b; the dimensions are about 5.2 × 4.9 × 9.6 nm^3 in the SDS−Al_2O_3 system (see runs A1 to A4 in Table S1) and about 5.2 × 4.9 × 10.8 nm^3 in the CTAB−SiO_2 system (see run B1 in Table S2). To simulate the formation of aggregates we employed a variable number of surfactants in a simulation box (see Figure S2 in the SI). The box dimensions are about 10.5 × 9.9 × 19 nm^3 in the SDS−Al_2O_3 system and about 10.25 × 9.9 × 20 nm^3 (see runs A5 to A10 Table S1) in the CTAB−SiO_2 system (see runs B2 to B8 in Table S2). We place N_s surfactant molecules uniformly distributed in the x−y plane with the heads pointing toward the solid surface. We allow about a 1 nm thick layer of water molecules between surfactant heads and the solid surface (see Figure S2a in the SI). We verified the reproducibility of our results using other initial conditions (see Figures S2a and S2b and Figure S7a and S7b in the SI). The composition of the SDS−alumina systems is given in runs A5 to A10 in Table S1, while that for the CTAB−silica systems is given in the runs B2 to B8 in Table S2. The simulation time is at least 80 ns; above this simulation time the density profiles do not change in two 10 ns consecutive intervals. Within this time scale we observe diffusion of molecules adsorbed on the substrate and aggregation of monomers adsorbed on the substrate. When the aggregates are adsorbed on the substrate surface, by diffusion they travel distances in the order of 1 nm in time intervals of 50 ns. In the aggregates the surfactant molecules exchange positions.

The free energy of adsorption is calculated through the potential of mean force (PMF) introduced by Kirkwood.[56] The negative of the gradient of the PMF gives the average force on the target atom as a function of the distance to the solid surface. We use umbrella sampling[57] to calculate the PMF. This technique overcomes limited sampling of energetically unfavorable configurations. The sampling is achieved by restraining the target molecule at a set of pre-established positions (windows) along the reaction coordinate (z-direction), then allowing the molecule to sample a large number of configurations in each window. The surfactant is restrained by means of a spring force applied on the sulfur (S) atom in SDS and on the nitrogen (N) atom in CTAB. To perform umbrella sampling simulations we generate a set of configurations at different separation distances between the surface and the surfactant headgroup. We use 36 windows for the umbrella sampling simulations of SDS on alumina (runs A1 to A4 in Table S1). At headgroup separation distances z < 0.4 nm from the solid surface the windows' spacing is 0.05 and 0.1 nm for $z \geq 0.4$ nm. The simulation time in each window is 10 ns. In runs A2 to A4 we allow formation of aggregates on the alumina surface prior to performing umbrella sampling simulations. We construct the surface with aggregates by placing N_s surfactant molecules uniformly distributed in the x−y plane and with the heads toward the solid surface: N_s = 12, 25, and 121 (runs A2 to A4 in Table S1). We allow a 1 nm thick layer of water molecules between surfactant heads and the solid surface. We run a 30 ns MD simulation to equilibrate the system. The set of initial configurations is generated by pulling a surfactant from the center of the aggregate to the bulk liquid phase; the pulling is applied through the sulfur headgroup atom. The umbrella sampling simulations in runs A2 to A4 are performed following the same protocol discussed above for the uncovered surface (run A1).

Umbrella sampling calculation of the CTAB−silica system is carried out using 42 windows of 0.05 and 0.1 nm (run B1 in Table S2). The movement of the surfactant headgroup is restrained in the z-direction by means of a harmonic potential; a spring constant of 2000 kJ mol^{-1} nm^{-2} is used. The molecule is allowed to move freely in the x- and y-directions, and in the z-direction the headgroup has only small variations around the initial position. The results of all windows are combined to obtain the PMF. Overlapping of the windows is the key to obtain a homogeneous sampling and reliable PMF. We use the weighted histogram analysis method (WHAM)[58] to obtain PMF with minimum error. The Krafft temperature is the minimum temperature required for micellization. Our simulations are performed at T = 298 K which is just above the Krafft temperature for CTAB and well above for SDS.[59,60] The temperature is controlled using the Nosé−Hoover thermostat.[61,62] We used the GROMACS simulation package version 16.1.[63−65] The code is run in a Linux environment (Ubuntu 16.1) using Tesla K40 and P100 GPU cards from Nvidia.

RESULTS

SDS Adsorption on α-Alumina. We first simulate the adsorption of a single SDS molecule on the alumina surface. Initially, the surfactant head is placed at about 0.8 nm from the solid surface with the tail up. We perform a 20 ns MD simulation run leaving the surfactant free to move. During the simulation time the surfactant may go away from the surface and return to it. Figure 2a shows the equilibrium density profiles of atoms and ions from the 20 ns MD simulation.

DOI: 10.1021/acs.jpcc.7b09466
J. Phys. Chem. C XXXX, XXX, XXX−XXX

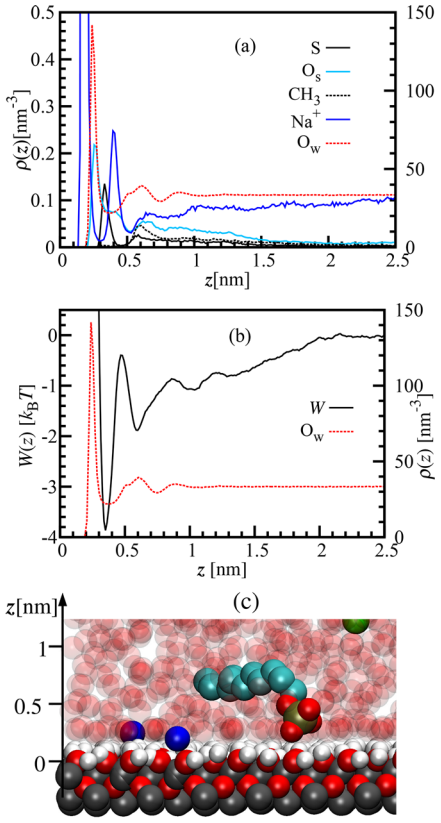

Figure 2. Adsorption of one SDS molecule on α-alumina (Run A1 in Table S1). (a) Free surfactant molecule. Density profiles of the sulfur (S) and oxygen (O_s) headgroup atoms, and the tail-end methyl group (CH_3) of SDS, the sodium ions in the solution, and the water oxygen atoms (O_w). The left scale is for S, O_s, CH_3, and Na^+, while the right scale is for O_w. (b) Potential of mean force (PMF) profile from umbrella sampling simulations for an SDS molecule pulled by the sulfur atom from the bulk solution to the alumina surface; the density profile of water oxygen atoms is shown for reference. (c) Surfactant configuration at the minimum of free energy. z = 0 is at the center of the outermost layer of alumina oxygen atoms. The color code is the same as in Figure 1.

The origin is set at the center of the outermost oxygen atom layer of alumina. The sodium ions (Na^+) are adsorbed at $z \approx$ 0.20 nm, replacing some adsorbed water molecules. Adsorption of salt ions has been reported onto other solid surfaces such as mica[66] in the presence of aqueous solution with NaCl. The water oxygen atoms (O_w) and the three oxygen atoms of the sulfate headgroup (O_s) are adsorbed at $z \approx$ 0.25 nm; the sulfate replaces water molecules from the first adsorbed layer. The peak of the sulfur atom profile is at about $z \approx$ 0.35 nm. The peak of adsorption of the tail-end methyl group is at $z \approx$ 0.6 nm. In the thermodynamic modeling literature,[67−69] various authors assume 0.55 nm layer of adsorbed water and ions between the surfactant head and solid surface. Our simulations show the adsorbed water molecules replaced by the surfactant head due to the strong electrostatic interaction between the charged surfactant head and the solid surface. Both the sodium ions and sulfate headgroups are adsorbed by releasing their hydration water and replacing the first adsorbed water layer. The density profiles of the oxygen and hydrogen of water are consistent with MD literature of water adsorption on the hydroxylated alumina surface.[70] Structured water is observed experimentally in the hydrated α-alumina (0001) surface. The oxygen of water in the first layer is at z = 0.23 nm, and ordering of water is extended to 1 nm into the bulk fluid, in agreement with experiments of refs 71 and 72, respectively.

Next, we examine the free energy of adsorption for a single SDS molecule on the alumina surface. The potential of mean force (PMF) is calculated with respect to the sulfur atom at the headgroup. Figure 2b portrays the PMF profile of an SDS molecule and density profile of water molecules. The PMF profile has three clear minima (at $z \approx$ 0.35, 0.6, and 1.0 nm) and then increases from about 1.3 to 2.1 nm, and it becomes constant for $z \gtrsim$ 2.1 nm. There is a free energy barrier of about ΔW = 0.35 k_BT for transferring the surfactant headgroup from the minimum at $z \approx$ 1 nm to the minimum at $z \approx$ 0.6 nm: in this location one layer of structured water is between the surfactant head and solid surface. A higher free energy barrier of about 1.6 k_BT has to be overcome to transfer the surfactant headgroup from z = 0.6 nm to the lowest free energy position at z = 0.35 nm. Based on the analysis of the density profiles and PMF, the surfactant is adsorbed on the alumina surface though the sulfate oxygen atoms and the tail lying on top of a water layer. Figure 2c shows one of the most likely configurations.

To examine the orientation of the surfactant molecule we trace the position of the tail-end methyl group (CH_3) when the headgroup is at a fixed position. In Figure 3 we analyze the position of the surfactant tail at different headgroup separation distances from the surface. At the minimum of the free energy profile (at z = 0.35 nm, Figure 3a) the probability of finding the tail lying on the first adsorbed layer of structured water is higher than in any other configuration. Similarly, when the headgroup is at z = 0.6, the 1 nm methyl group is found adsorbed next to the first structured water layer (Figures 3b and 3c). The first layer of structured water at z = 0.25 nm is in-between the methyl group and solid surface. As mentioned above, the tail of SDS does not replace the adsorbed water. At z = 1.3 nm the tail adsorption on the structured water layer decreases. From $z \gtrsim$ 1.6 nm the head is sufficiently far from the surface, and the tail is symmetrically distributed around the head (see Figures 3(e) and (f)); there is no preferential location of the surfactant tail.

To investigate formation of different structures we compute the free energy of transferring one SDS surfactant molecule from the bulk to the alumina surface covered with surfactant aggregates. As mentioned above, the aggregates are built by placing N_s surfactant molecules uniformly distributed in the $x-y$ plane and simulated for 30 ns. The aggregates are made of N_s = 12, 25, and 121 surfactant molecules (runs A2 to A4 in Table S1). Figure 4 shows the PMF profile and snapshot of the aggregates: in (a) and (b) the aggregate is made of N_s = 12 surfactants, in (c) and (d) N_s = 25, and N_s = 121 in (e) and (f). The PMF profiles have similar characteristics, that is, a plateau when the headgroup is away from the aggregate surface, a free energy drop when the tail comes into contact with the adsorbed aggregate, a slow varying interval when the headgroup enters into the aggregate, and a free energy minimum. For the smallest aggregate (N_s = 12), the surfactant comes into contact with the aggregates at about $z \approx$ 3 nm (see Figure 4a). When the aggregates are made of N_s = 25 and N_s = 121 surfactants the contact occurs at $z \approx$ 3.5 nm and at $z \approx$ 4 nm, respectively (see Figures 4b and 4c). The slow varying region extends more in the z-direction as the aggregate number increases. For N_s = 12 and 25 the PMF profiles have a local minimum at $z \approx$ 0.6 nm and a maximum at $z \approx$ 0.5 nm. For N_s = 121 the PMF profile decreases to an absolute minimum and shows two shoulders at $z \approx$ 0.5 and 0.8 nm. For the three aggregate sizes

DOI: 10.1021/acs.jpcc.7b09466
J. Phys. Chem. C XXXX, XXX, XXX−XXX

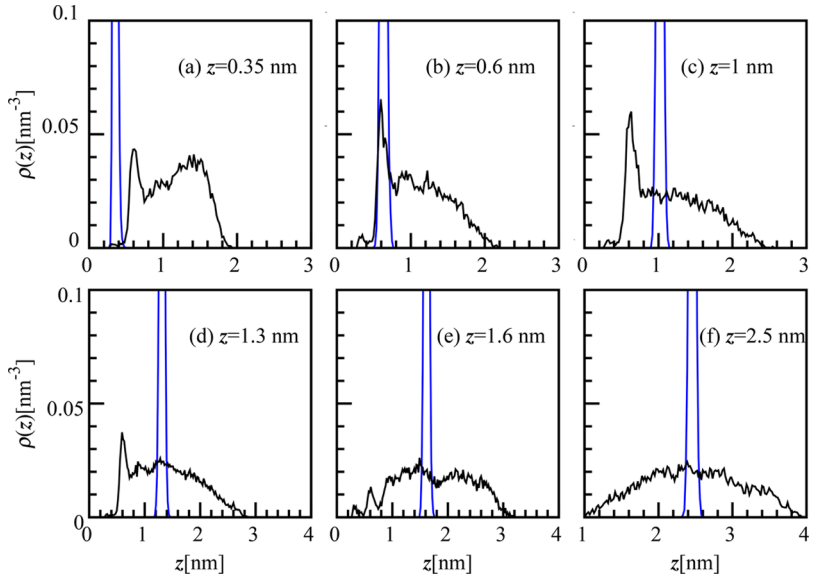

Figure 3. Adsorption of the SDS hydrocarbon tail on the alumina surface (Run A1 in Table S1). Density profiles of the sulfur headgroup atom (blue line) and the tail-end methyl group (black line) of SDS. The sulfur atom is kept fixed at different separation distances from the alumina surface: (a) $z \approx 0.35$ nm, (b) $z \approx 0.6$ nm, and (c) $z \approx 1.0$ nm correspond to the first, second, and third PMF minima, respectively (see Figure 2b); (d) $z \approx 1.3$ nm and (e) $z \approx 1.6$ nm are in the region where the PMF has a constant slope, and (f) $z \approx 2.5$ nm is at the PMF flat region (see Figure 2b).

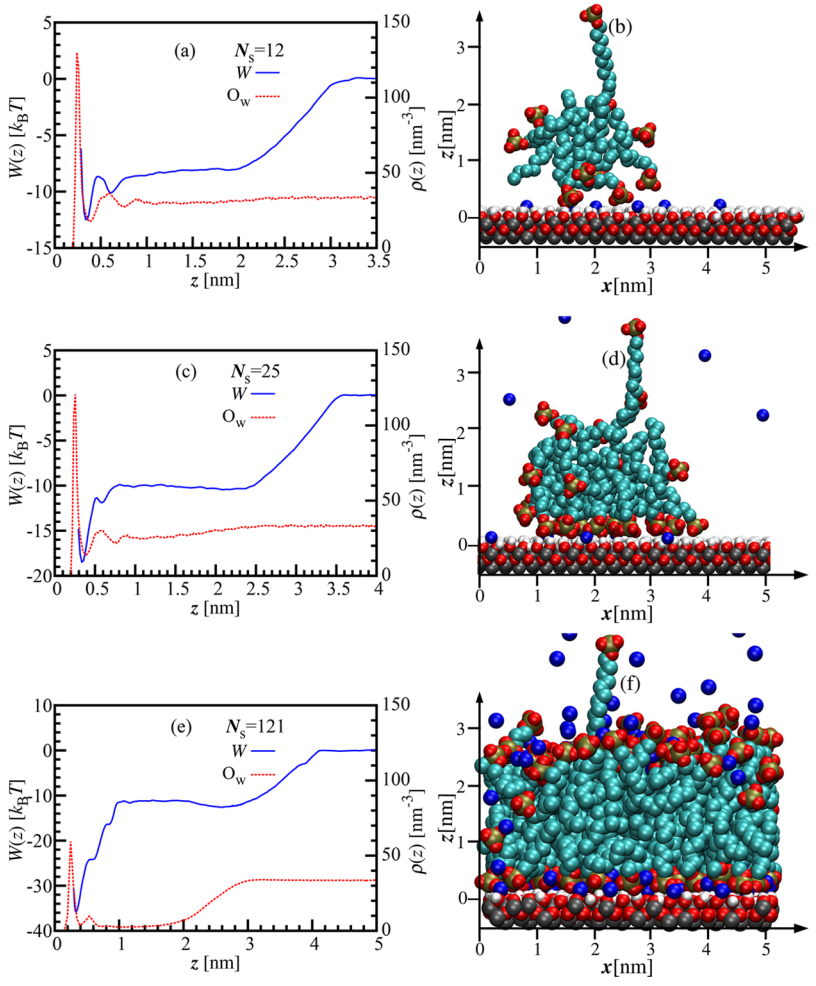

Figure 4. Free energy of transferring one SDS surfactant molecule from the bulk solution to the alumina surface with adsorbed SDS aggregates. Left (a,c,e): Potential of mean force (blue line) and density profile of water oxygen atoms (red line). Right (b,d,f): Snapshot of the adsorbed aggregate on the substrate and the pulled surfactant molecule; (a) and (b) are from run A2, (c) and (d) from run A3, and (e) and (f) from run A4 in Table S1. The color code is the same as in Figure 1.

DOI: 10.1021/acs.jpcc.7b09466
J. Phys. Chem. C XXXX, XXX, XXX−XXX

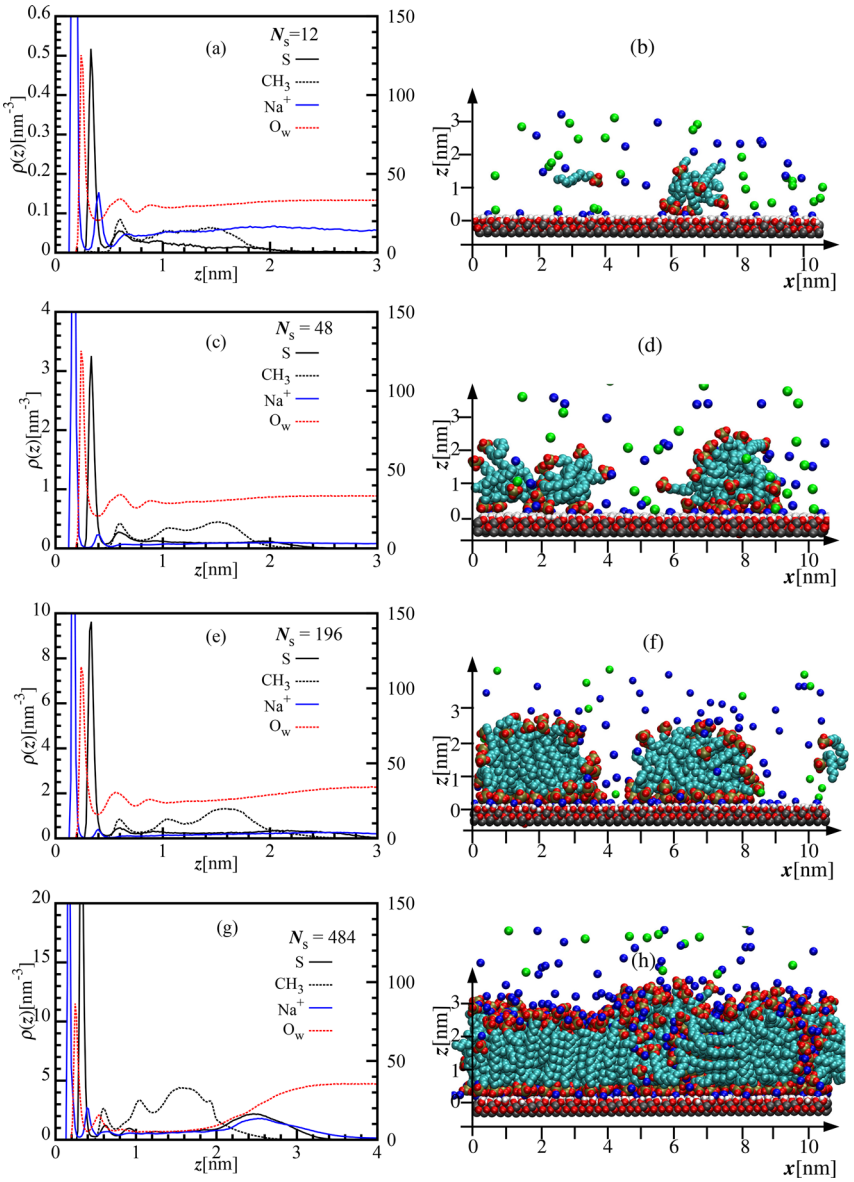

Figure 5. Structures of SDS surfactant molecules adsorbed on alumina. Left (a,c,e,g): Density profiles of the sulfur (S) headgroup atoms and tail-end methyl groups (CH_3) of the SDS molecules, the sodium ions Na^+ in the solution, and the water oxygen atoms (O_w). Right (b,d,f,h): Snapshot of the SDS aggregates adsorbed on the alumina surface; (a) and (b) are from run A5 (N_s = 12), (c) and (d) from run A7 (N_s = 48), (e) and (f) from run A9 (N_s = 196), and (g) and (h) from run A10 (N_s = 484) in Table S1. The color code is the same as in Figure 1.

the absolute minimum is located at $z \approx 0.35$ nm like in the surface free of aggregates (see Figure 2b). The free energy minimum is about −12, −18, and −35 kJ/mol for N_s = 12, 25, and 121, respectively. When the alumina surface is free from adsorbed surfactants the free energy minimum is about −3.8 kJ/mol (see Figure 1b). The surfactant adsorption becomes more favorable as the aggregate size increases. This result suggests a connection with the steep increase in the experimental adsorption; the increase could be due to increased tail−tail interaction.

The water oxygen density profile shows a peak at $z \approx 0.25$ nm, a local minimum at $z \approx 0.4$ nm, and a second maximum at $z \approx 0.6$ nm. The density profiles do not change significantly when the aggregates are made of 12 and 25 surfactant molecules; however, an important reduction of the adsorption peak is observed for aggregates of N_s = 121. Water is nearly depleted from the bilayer region at 0.4 nm $\lesssim z \lesssim$ 3 nm.

We investigate the morphology of the aggregates as a function of the surfactant concentration (runs A5 to A10 in Table S1). As explained above, the surfactants are initially distributed in the x−y planes, uniformly, perpendicular to the solid surface, and with the headgroups pointing toward the substrate. We analyze the density profiles of the sulfur headgroup atoms (S), the tail-end methyl groups (CH_3), the sodium ions (Na^+), and the water oxygen atoms (O_w). Figure 5 shows the density profiles (right) and a snapshot of an equilibrium configuration (left): N_s = 12 in (a) and (b); N_s = 48 in (c) and (d), N_s = 196 in (e) and (f), and N_s = 484 in (g) and (h). Other results from our simulation runs are presented in Figure S4 in the SI.

The sulfur (S) and Na^+ density profiles have a main peak at $z \approx 0.35$ and 0.2 nm, respectively; the height of the adsorption peak increases as the number of surfactants in the system N_s increases. At low surfactant concentration ($N_s \lesssim 48$) the

DOI: 10.1021/acs.jpcc.7b09466
J. Phys. Chem. C XXXX, XXX, XXX−XXX

Table 1. Adsorption of SDS on α-Alumina from MD Simulations[a]

N_s	Γ_s [molecules/nm^2]	n_a	$\bar{n}_a$	A [nm^2]	l [nm]	morphology
12	0. 08	1−6	2.6	1.8	1.5	hemimicelle
28	0. 21	1−12	7.3	3	1.7	hemimicelle
48	0. 39	8−14	13.6	3−4.5	1.65	hemimicelle-bilayer
128	1. 01	11−33	20.8	3−7.5	1.8	hemimicelle-bilayer
196	1. 20	15−47	31	3.5−13.5	1.9	bilayer
484	4.65	484	484	96	2.8	bilayer

[a] N_s is the number of surfactant molecules in the simulation box; Γ_s is the adsorption; n_a is the aggregation number; $\bar{n}_a$ is the mean aggregation number; A is the area covered per aggregate; and l is the mean aggregate thickness. The right-most column gives a brief description of the aggregate morphology.

adsorbed surfactants are facing toward the alumina surface. As N_s increases, a maximum is developed in the sulfur density profiles at $z \gtrsim 2.1$ nm (see Figures 5e and 5g). This maximum represents the headgroup accumulation in a second layer away from the solid surface. The density profiles of the tail-end methyl groups (CH_3) show the hydrocarbon region within 0.3 nm $\lesssim z \lesssim$ 2 nm. As N_s increases the height of the CH_3 density profiles increases at around $z \approx 1.8$ nm, indicating a higher surfactant tail packing. The water density profile has a main adsorption peak at $z \approx 2.5$ nm. As N_s increases, the height of the water adsorption peak decreases due to the water displacement by the surfactant headgroups and Na^+ ions. Water is strongly depleted from the bilayer region at the highest surfactant adsorption (see Figure 5g).

The snapshots in Figure 5 (right side) display the morphology of the SDS aggregates adsorbed on α-alumina from our MD simulations. The main properties of the aggregates are summarized in Table 1. Most of the surfactants in the aggregates formed at low surfactant adsorption are facing toward the substrate, and the tails are pointing upward (see Figures 5b and 5d and Figure S3a and S3b in the SI); these aggregates are called hemimicelles. At higher surfactant adsorption the substrate coverage is by aggregates with bilayer structure (see Figures 5f and Figures S3c and S4d in the SI). At N_s = 484 a single bilayer is formed (see Figure 5h and Figure S3d in the SI). The morphologies of the aggregates in our MD simulations are in agreement with the structures in the four-region isotherm model:[15−17] in region I the surfactant molecules are adsorbed as monomers; in region II the surfactant molecules form hemimicelles (see Figure 5b and 5d); in region III the aggregates possess the structure of a bilayer (see Figures 5f and Figure S4d in the SI); and in region IV the substrate is covered by a surfactant bilayer (see Figure 5h). The mean aggregation number ($\bar{n}_a$), the mean area per aggregate (A), and the thickness (l) of the surfactant layer increase with the surfactant adsorption (Γ_s) (see Table 1). At the highest surfactant adsorption about 96% of the surface is covered by a continuous bilayer. The adsorption layer thickness is about 1.5 and 2.8 nm at the at the lowest and highest adsorption, respectively.

From positron annihilation spectroscopy measurements the hydrocarbon core radius of SDS micelles in aqueous solution is estimated to be between 1.19 and 1.5 nm. By taking into account the size of the polar sulfate group the total SDS micelle radius is about 1.8 nm.[73] Small-angle neutron scattering (SANS) and small-angle X-ray scattering (SAXS) experiments[74−76] reveal spheroidal geometry (oblate and prolate) of the SDS micelles in bulk. The spheroids are characterized by the minor and major axis lengths a and b, respectively. The minor axis length is usually found to be between 75 and 90% of the length of a fully extended surfactant hydrocarbon tail.

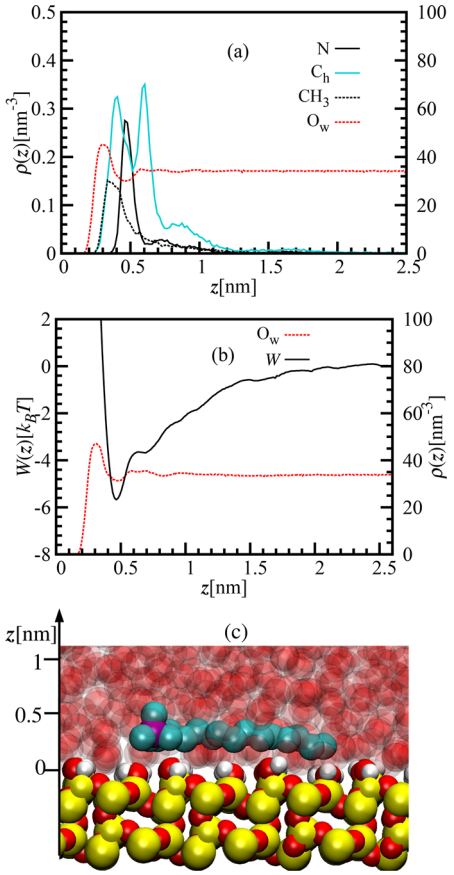

Figure 6. Adsorption of one CTAB molecule on silica (Run B1 in Table S2). (a) Free surfactant molecule. Density profiles of the nitrogen atoms (N), methyl (C_h) headgroups, and tail-end methyl groups (CH_3) of CTAB, and the water oxygen atoms (O_w). The left scale is for C_h, N, and CH_3, while the right scale is for O_w. (b) Potential of mean force (PMF) profile from umbrella sampling simulations for a CTAB molecule pulled by the nitrogen atom from the bulk solution to the silica surface; the density profile of oxygen atoms of water molecules is shown for reference. (c) Surfactant configuration at the minimum of free energy. z = 0 is at the center of the outermost oxygen layer of silica. The color code is the same as in Figure 1.

Along the major axis direction (b-direction), the aggregate size increases at higher electrolyte and surfactant concentration and may be significantly elongated. In our MD simulations, the length of the fully extended SDS hydrocarbon tail is about 1.52 nm from the center of the first carbon to the center of the end carbon. In the SDS adsorbed aggregates from our MD simulations, the hydrocarbon region is about 1.5 nm in hemimicelles and about 2 nm in the bilayer geometry. Next to

DOI: 10.1021/acs.jpcc.7b09466
J. Phys. Chem. C XXXX, XXX, XXX−XXX

the substrate, the sulfur headgroup atoms are strongly localized within a layer of about 0.2 nm. In the region next to the aqueous phase in the bilayer aggregates, the sulfur atoms are distributed within a layer of about 0.8 nm.

CTAB Adsorption on Silica. Now we investigate the adsorption of CTAB surfactant on silica. First we simulate the adsorption of a single free surfactant molecule with the conditions in run B1 in Table S2. Figure 6a shows the equilibrium density profiles when the surfactant is adsorbed. Initially, the surfactant head is placed at about 1 nm away from the solid surface. The origin is located at the center of the outermost oxygen layer of silica. The water oxygen atoms (O_w) adsorbed on the silica surface are located at $z \approx 0.3$ nm. Water adsorption is stronger on α-alumina than on silica: the adsorption peak is about 140 nm^{-3} for alumina (see Figure 2a) and about 50 nm^{-3} for silica (see Figure 6a). The three methyl groups of the surfactant head (C_h) are adsorbed at $z \approx 0.35$ and 0.65 nm indicating two C_h groups close to the surface, while the other group is away. The adsorption peak of the nitrogen headgroup atom is at $z \approx 0.5$ nm. The peak of the tail-end methyl group is at $z \approx 0.35$ nm indicating the adsorption slightly above the water oxygen layer at $z \approx 0.35$ and at the same distance as the two adsorbed methyl headgroups. Figure 6b portrays the PMF profile for the headgroup nitrogen atom of the CTAB molecule and the density profile of water molecules. The PMF profile has a clear minimum close to $z \approx 0.5$ nm and a flat region at $z \approx 0.6$ nm from where the PMF profile increases and is zero from $z \approx 2.4$ nm. Figure 6c shows the most likely configuration of the surfactant adsorbed on silica, lying on the surface slightly above the adsorbed water layer. The adsorbed methyl and methylene groups are nearly at the same distance from the surface. A configuration with the surfactant tail perpendicular to the substrate is very unlikely, ruling out the formation of monolayers.

The adsorption of SDS on alumina is significantly different from the adsorption of CTAB on silica. On alumina, the SDS oxygen headgroup atoms are adsorbed at the same distance as the first water layer, and the tail-end methyl group is on top of the first water layer (see Figure 2c). On silica, both the head and tail methyl groups of CTAB are adsorbed nearly at the same position as the first water layer. The surfactant free energy of adsorption (at the absolute minimum) in the SDS−alumina system is about $-3.8\ k_BT$ and about $-5.8\ k_BT$ in the adsorption of CTAB on silica. CTAB on silica has a lower free energy of adsorption than SDS on alumina (about 2 k_BT) due to a stronger contribution from the tail.

The CTAB tail adsorption is investigated in Figure 7 by examining the density profile of the tail-end methyl group (CH_3) when the surfactant headgroup is located at different separation distances from the surface. When the CTAB headgroup is close to the substrate there is a high probability to find the tail adsorbed on the substrate as can be seen in Figures 7a, 7b, and 7c with the nitrogen headgroup atom at z = 0.5, 0.7, and 1.1 nm, respectively. At higher separation distances there is a probability of finding the tail in the liquid phase (see Figure 7d). When the head is sufficiently far from the surface the tail is symmetrically distributed around the head (see Figures 7(e) and (f)). The tail density profile $\rho(z)$ is directly related to the tail free energy of adsorption $W_c(z)$ by $\rho(z) \sim \exp\{-W_c(z)/k_BT\}$. The maximum of the tail density profile is about 0.06 nm^{-3} for SDS-alumina (see Figure 3c), whereas it is about 0.2 nm^{-3} for CTAB-silica (see Figure 7a). This implies a lower free energy of adsorption of the hydrocarbon tail adsorbed on silica than on alumina. For the silica surface, the hydrocarbon tail is adsorbed just above the first adsorbed water layer. As discussed above, water is more strongly adsorbed on α-alumina than on silica.

In Figure 8 we investigate the morphology of the aggregates as a function of the concentration of surfactant molecules (runs B2 to B8 in Table S2). We analyze the density profiles of the nitrogen headgroup atoms (N), the tail-end methyl groups (CH_3), and the water oxygen atoms (O_w). Figure 8 shows the density profiles (right) and a snapshot of an equilibrium configuration (left): N_s = 12 in (a) and (b), N_s = 96 in (c) and (d), N_s = 196 in (e) and (f), and N_s = 360 in (g) and (h). Other results from our simulations run are presented in

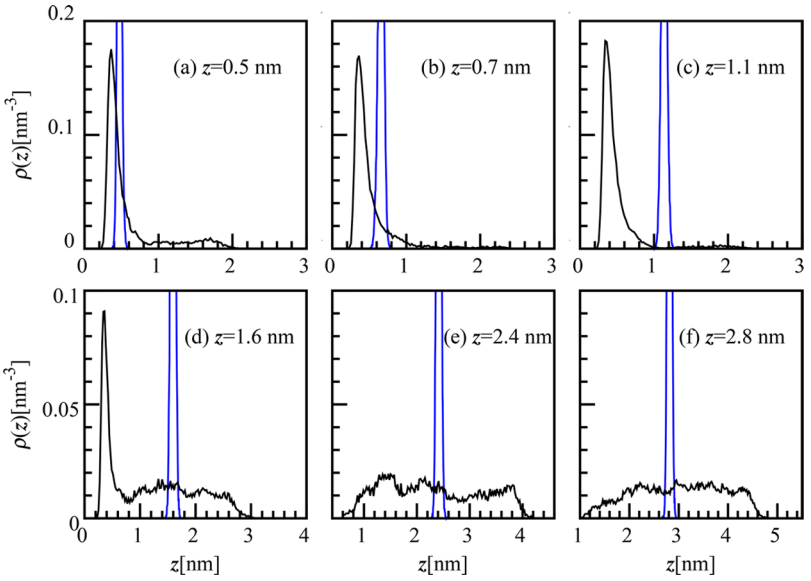

Figure 7. Adsorption of the CTAB hydrocarbon tail on the silica surface (Run B1 in Table S2). Density profiles of the nitrogen headgroup atom (blue line) and the tail-end methyl group of CTAB. The nitrogen atom is kept at different separation distances from the silica surface: (a) $z \approx 0.5$ nm corresponds to the position of the PMF minimum (see Figure 6b), (b) $z \approx 0.7$ nm, (c) $z \approx 1.1$ nm, (d) $z \approx 1.6$ nm, (e) $z \approx 2.4$ nm, and (f) $z \approx 2.8$ nm.

DOI: 10.1021/acs.jpcc.7b09466
J. Phys. Chem. C XXXX, XXX, XXX−XXX

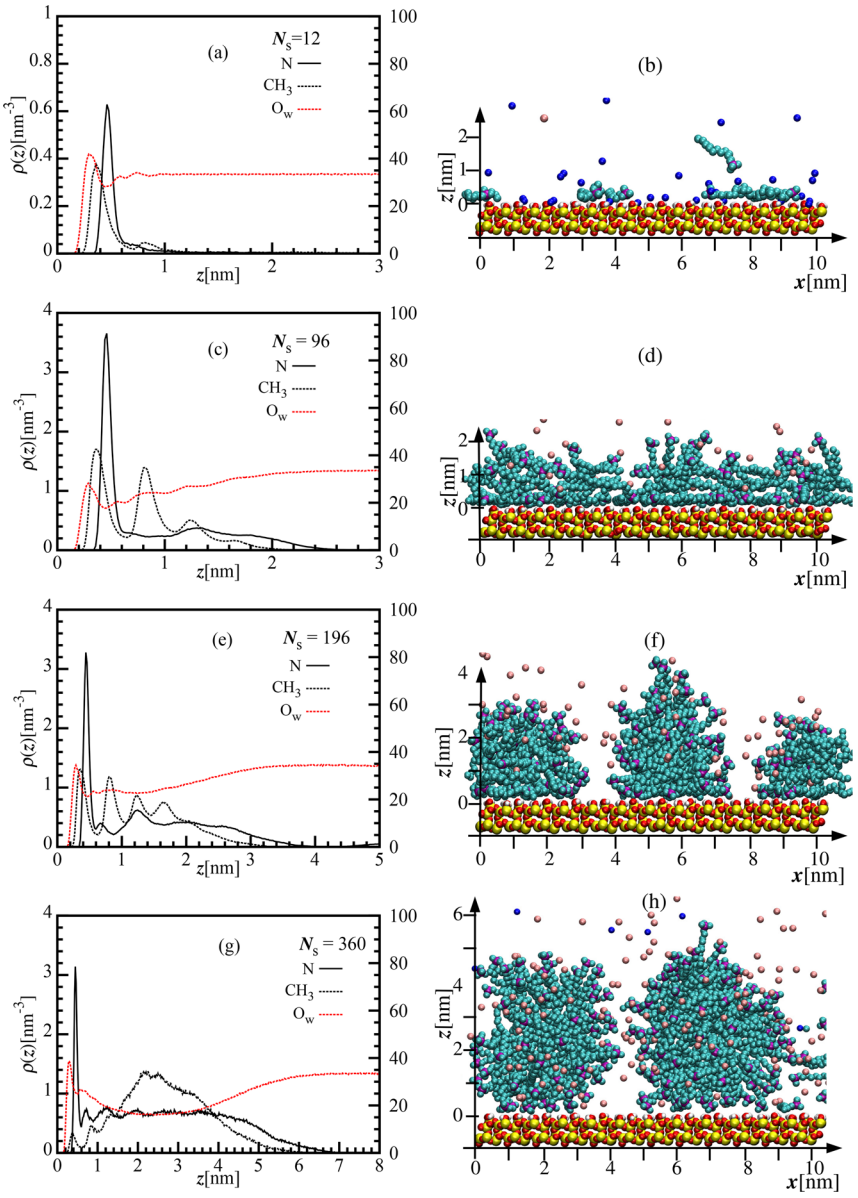

Figure 8. Structures of CTAB surfactant molecules adsorbed on silica. Left (a,c,e,g): Density profiles of the nitrogen (N) headgroup atoms and tail-end methyl (CH_3) groups of the CTAB molecules and the water oxygen atoms (O_w). Right (b,d,f,h): Snapshot of the CTAB aggregates adsorbed on the silica surface. (a) and (b) are from run B2 (N_s = 12), (c) and (d) from run B5 (N_s = 96), (e) and (f) from run B7 (N_s = 196), and (g) and (h) from run B8 (N_s = 360) in Table S2. The color code is the same as in Figure 1.

Table 2. Adsorption of CTAB on Silica from MD Simulations[a]

N_s	Γ_s [molecs./nm^2]	n_a	$\bar{n}_a$	A [nm^2]	l [nm]	morphology
12	0.12	1–2	1.5	n/a	0.3	flat
28	0.24	1–5	3	2.1–4.2	0.3	flat
64	0.52	4–14	7.5	4–9	1.0	hemimicelle
96	0.80	8–21	11.2	4–11	1.8	hemimicelle
128	0.87	12–24	20.2	7–13	1.9	hemimicelle
196	1.38	16–44	35	7–14.5	3.1	hemimicelle
360	3.54	80–93	86.5	13.5–18.5	5.0	micelle

[a] N_s is the number of surfactant molecules in the simulation box; Γ_s is the adsorption; n_a is the aggregation number; $\bar{n}_a$ is the mean aggregation number; A is the area covered per aggregate; and l is the mean aggregate thickness. The right-most column provides a brief description of the aggregate morphology.

Figure S6 in the SI. The density profile of the nitrogen (N) atom has an adsorption peak at $z \approx 0.5$ nm; the range of the density profile increases as the number of adsorbed surfactants N_s increases. The peak height is 0.6 nm^{-3} for N_s = 12 and about 3.2 nm^{-3} for $N_s \geq 64$. This is an indication of saturation of the surface by surfactant headgroup adsorption. The density profile

DOI: 10.1021/acs.jpcc.7b09466
J. Phys. Chem. C XXXX, XXX, XXX−XXX

of the tail-end methyl group (CH_3) has a peak at $z \approx 0.4$ nm; by increasing the concentration of surfactant molecules and for $N_s < 128$ the height of the adsorption peak increases and decreases at $N_s > 128$. This is an indication of the structural change of the adsorbed aggregates. The snapshot at the right side displays the morphology of the aggregates. At $N_s = 12$ most of the adsorbed surfactant monomers lie on the substrate (see Figure 8b and Figure S5a in the SI). At higher concentration the surfactants form aggregates of molecules stacking on other molecules; most of the surfactants are still lying on the substrate (see Figure 8d and Figure S5b in the SI). At $N_s = 196$ hemimicelles form with the surfactant on the top making hemispherical shape and the surfactants on the bottom extended on the substrate (see Figure 8f and Figure S5c in the SI). At the highest number of surfactants the aggregates are full micelles (see Figure 8h and Figure S5d in the SI). The main properties of the CTAB aggregates adsorbed on silica are summarized in Table 2. The mean aggregation number ($\bar{n}_a$), the mean area per aggregate (A), and the thickness (l) of the surfactant layer increase with the surfactant adsorption (Γ_s) (see Table 1). The aggregation number of the micelles at the highest surfactant concentration (86.5) is in agreement with the experimental value from fluorescent probe studies.[22] The aggregate thickness has strong variations associated with structural changes: the aggregates are flat in the range of 0.3 nm $\lesssim l \lesssim$ 1 nm; at 1.8 nm $\lesssim l \lesssim$ 3 nm the aggregates are hemimicelles; and $l \approx 5$ nm represents full micelles of overall radius about 2.5 nm. In neutron reflection experiments the thickness of the adsorbed aggregates is estimated to be 3.2 nm[26] which corresponds to the observed aggregate thickness in hemimicelles (see Figures 8e and 8f). In our MD simulations the structure of the CTAB aggregates adsorbed on silica substrate is always discontinuous as observed in AFM studies.[21]

In bulk, prolate ellipsoidal micelles of CTAB are found by means of SANS.[77,78] From the measurements the aggregation number is estimated between 127 and 152 molecules; the micelle hydrocarbon core radius is about 2.5 nm; and the overall radius is about 2.9 nm. In our MD simulations, the CTAB fully extended hydrocarbon chain length is about 2.0 nm and is equal to the hydrocarbon core radius of the adsorbed micelles at the silica surface (see Figure 8h).

Major differences are observed in the structures adsorbed on the two substrates. Hemimicelles in the SDS−alumina system are formed with the surfactant head facing the substrate and the tail pointing toward the liquid phase. In the CTAB−silica system, the hemimicelle surfactants are lying on the surface of silica, and other surfactant headgroups are pointing toward the liquid phase forming the hemispherical shape. At higher concentration, a bilayer structure is formed in the SDS−alumina system even when the surface coverage is discontinuous. At the highest adsorption the bilayer structure is continuous. The CTAB−silica system goes from hemimicelles to full micelles by increasing the surfactant concentration. The coverage of the silica substrate is discontinuous.

To verify the reproducibility of our results we run our simulations employing two different initial conditions of the surfactants. Figure S2a shows the typical initial condition with the surfactants aligned perpendicular to the solid surface and uniformly distributed in the $x-y$ plane. Figure S2b shows a random initial configuration of the surfactant. In both systems the number of surfactant molecules is $N_s = 128$ (see run B6 in Table S2). The density profiles and a snapshot of the final configuration are presented in Figures S6e, S6f, S6g, and S6h. We observe similar results from both simulations. The shape, the peak location, and peak height of the density profiles are similar in Figures S6e and S6g. The aggregates from both simulations are hemimicelles (S6f and S6h).

Another example where we used two different initial conditions for the surfactants is presented in Figure S7. In Figure S7a the surfactant molecules are uniformly distributed in the $x-y$ plane and aligned perpendicular to the solid surface. In Figure S7b the surfactant forms two layers in the $x-y$ plane, and the headgroups meet at the middle of the bilayer. In both simulations the surfactant forms spherical micelles (see Figure S7c and Figure S7d).

The picture of CTAB adsorption on silica has gradually evolved. Early studies based on the adsorption isotherm measurements suggested the adsorption of a monolayer at low concentration and a bilayer at high concentration.[23] In later experiments the substrate coverage by the surfactant is not continuous but in the form of discrete aggregates.[18−22,25,26,79] The aggregates are modeled as spherical structures with surfactant headgroups facing both toward the substrate and into solution.[20,80] These structures were first called hemimicelles and later renamed as admicelles. Spherical aggregates, worm-like structures, and short rods are observed using atomic force microscopy.[80−82] Our molecular dynamics results show discrete aggregates in agreement with the experiments. At low surfactant adsorption we observe single and small groups of surfactants lying on the substrate. Hemimicelles form at higher surfactant concentration. The hemimicelles observed in our simulations have some surfactant molecules lying on the substrate, and the headgroup of other surfactant molecules is pointing in the opposite direction of the surface. Fully adsorbed micelles are seen at the highest concentration. The functionality of the silica surface is likely to be very important as different treatments applied in experiments can change the proportion of siloxane, silane, and silanol groups on silica as well as the different types of silica, namely, hydrophobic, hydrophilic, crystalline, and amorphous. Therefore, adsorption of surfactants on silica may not fit a into a simple picture.

CONCLUSIONS

We investigate the adsorption mechanisms, structure, and morphology of ionic surfactants on mineral surfaces using molecular dynamics simulations in two different systems: (1) SDS on alumina and (2) CTAB on silica. Our study is performed as a function of the surfactant concentration. The structure and morphology of the aggregates are determined to a great extent by how the substrate interacts with ions and water.

In the SDS−alumina system we highlight the following:

- Water molecules and Na^+ ions are strongly adsorbed on alumina leading to a weak binding and random orientation of the SDS surfactant tail.
- The SDS headgroup is attracted by the outermost hydrogen atoms on the substrate and by the adsorbed Na^+ counterions; the headgroup may remove structured water and come in direct contact with the hydroxyl groups of alumina.
- As the number of adsorbed surfactant molecules increases we observe single adsorbed molecules, hemimicelles, and bilayers. When a single SDS molecule is adsorbed on alumina, the tail has a random orientation with some preference to lie on the water layer adsorbed on alumina.

DOI: 10.1021/acs.jpcc.7b09466
J. Phys. Chem. C XXXX, XXX, XXX−XXX

- As the aggregate size increases the surfactant free energy of adsorption significantly decreases. Our results suggest that adsorption is driven by the tail−tail interaction as the aggregate size increases.

In the CTAB−silica system we highlight the following:

- The cationic CTAB headgroup is electrostatically attracted by the negatively charged oxygen atoms of silica.
- There is a strong binding of the surfactant tail displacing the weakly adsorbed water molecules.
- As the surfactant concentration increases we find single and small groups of surfactant molecules lying on the substrate, hemimicelles, and micelles.
- At low surfactant coverage electrostatic attraction is the main driving force of the surfactant headgroup adsorption. When the aggregates form on the substrate the tail−tail interaction takes a central role in the surfactant adsorption.

The water−surface interaction, the configuration of the adsorbed tail, and the tail−tail interaction play fundamental roles, under certain conditions as important as the electrostatic interactions.

■ ASSOCIATED CONTENT

Supporting Information

The Supporting Information is available free of charge on the ACS Publications website at DOI: 10.1021/acs.jpcc.7b09466.

Tables of the setup composition and force field parameters and additional simulation data (PDF)

■ AUTHOR INFORMATION

Corresponding Author

*E-mail: abbas.firoozabadi@yale.edu. Phone: +1 (650)326-9172. Fax: +1 (650) 472-9285.

ORCID

Abbas Firoozabadi: 0000-0001-6102-9534

Notes

The authors declare no competing financial interest.

■ ACKNOWLEDGMENTS

We acknowledge the financial support of ExxonMobil and the member companies of the RERI research consortium. We thank Dr. Arben Jusufi of ExxonMobil for his interest and comments on different parts of the work.

■ REFERENCES

(1) Rosen, M. J.; Kunjappu, J. T. *Surfactants and Interfacial Phenomena*, 4th ed.; John Wiley & Sons: Hoboken, NJ, 2012.

(2) Bai, B.; Hankins, N. P.; Hey, M. J.; Kingman, S. W. In Situ Mechanistic Study of SDS Adsorption on Hematite for Optimized Froth Flotation. *Ind. Eng. Chem. Res.* **2004**, *43*, 5326−5338.

(3) Hirasaki, G. J.; Miller, C. A.; Puerto, M. Recent Advances in Surfactant EOR. SPE Annual Technical Conference and Exhibition. 2008.

(4) Hamme, J. D. V.; Singh, A.; Ward, O. P. Physiological Aspects: Part 1 in a Series of Papers Devoted to Surfactants in Microbiology and Biotechnology. *Biotechnol. Adv.* **2006**, *24*, 604−620.

(5) Singh, A.; Hamme, J. D. V.; Ward, O. P. Surfactants in Microbiology and Biotechnology: Part 2. Application Aspects. *Biotechnol. Adv.* **2007**, *25*, 99−121.

(6) López-Montilla, J. C.; Pandey, S.; Shah, D. O.; Crisalle, O. D. Removal of Non-Ionic Organic Pollutants from Water Via Liquid-Liquid Extraction. *Water Res.* **2005**, *39*, 1907−1913.

(7) Adak, A.; Bandyopadhyay, M.; Pal, A. Removal of Crystal Violet Dye From Wastewater by Surfactant-Modified Alumina. *Sep. Purif. Technol.* **2005**, *44*, 139−144.

(8) Bohmer, M. R.; Koopal, L. K.; Janssen, R.; Lee, E. M.; Thomas, R. K.; Rennie, A. R. Adsorption of Nonionic Surfactants on Hydrophilic Surfaces. An Experimental and Theoretical Study on Association in the Adsorbed Layer. *Langmuir* **1992**, *8*, 2228−2239.

(9) McDermott, D. C.; Lu, J. R.; Lee, E. M.; Thomas, R. K.; Rennie, A. R. Study of the Adsorption from Aqueous Solution of Hexaethylene Glycol Monododecyl Ether on Silica Substrates Using the Technique of Neutron Reflection. *Langmuir* **1992**, *8*, 1204−1210.

(10) Lee, E. M.; Thomas, R. K.; Cummins, P. G.; Staples, E. J.; Penfold, J.; Rennie, A. R. Determination of the Structure of a Surfactant Layer Adsorbed at the Silica/Water Interface by Neutron Reflection. *Chem. Phys. Lett.* **1989**, *162*, 196−202.

(11) Grant, L. M.; Tiberg, F.; Ducker, W. A. Nanometer-Scale Organization of Ethylene Oxide Surfactants on Graphite, Hydrophilic Silica, and Hydrophobic Silica. *J. Phys. Chem. B* **1998**, *102*, 4288−4294.

(12) Schrödle, S.; Richmond, G. L. Equilibrium and Non-Equilibrium Kinetics of Self-Assembled Surfactant Monolayers: A Vibrational Sum-Frequency Study of Dodecanoate at the Fluorite-Water Interface. *J. Am. Chem. Soc.* **2008**, *130*, 5072−5085.

(13) Jang, W.-H.; Drelich, J.; Miller, J. D. Wetting Characteristics and Stability of Langmuir-Blodgett Carboxylate Monolayers at the Surfaces of Calcite and Fluorite. *Langmuir* **1995**, *11*, 3491−3499.

(14) Becraft, K. A.; Richmond, G. L. Surfactant Adsorption at the Salt/Water Interface: Comparing the Conformation and Interfacial Water Structure for Selected Surfactants. *J. Phys. Chem. B* **2005**, *109*, 5108−5117.

(15) Somasundaran, P.; Fuerstenau, D. W. Mechanisms of Alkyl Sulfonate Adsorption at the Alumina-Water Interface. *J. Phys. Chem.* **1966**, *70*, 90−96.

(16) Somasundaran, P.; Kunjappu, J. T. In-situ Investigation of Adsorbed Surfactants and Polymers on Solids in Solution. *Colloids Surf.* **1989**, *37*, 245−268.

(17) Fan, A.; Somasundaran, P.; Turro, N. J. Adsorption of Alkyltrimethylammonium Bromides on Negatively Charged Alumina. *Langmuir* **1997**, *13*, 506−510.

(18) Gao, Y.; Du, J.; Gu, T. Hemimicelle Formation of Cationic Surfactants at the Silica Gel-Water Interface. *J. Chem. Soc., Faraday Trans. 1* **1987**, *83*, 2671−2679.

(19) Gu, T.; Huang, Z. Thermodynamics of Hemimicellization of Cetyltrimethylammonium Bromide at the Silica Gel/Water Interface. *Colloids Surf.* **1989**, *40*, 71−76.

(20) Gu, T.; Rupprecht, H. Hemimicelle Shape and Size. *Colloid Polym. Sci.* **1990**, *268*, 1148−1150.

(21) Howard, S. C.; Craig, V. S. J. Adsorption of the Cationic Surfactant Cetyltrimethylammonium Bromide to Silica in the Presence of Sodium Salicylate: Surface Excess and Kinetics. *Langmuir* **2009**, *25*, 13015−13024.

(22) Ström, C.; Hansson, P.; Jönsson, B.; Söderman, O. Size of Cationic Surfactant Micelles at the Silica-Water Interface: A Fluorescent Probe Study. *Langmuir* **2000**, *16*, 2469−2474.

(23) Bijsterbosch, B. Characterization of Silica Surfaces by Adsorption from Solution. Investigations into the Mechanism of Adsorption of Cationic Surfactants. *J. Colloid Interface Sci.* **1974**, *47*, 186−198.

(24) Paria, S.; Khilar, K. C. A Review on Experimental Studies of Surfactant Adsorption at the Hydrophilic Solid-Water Interface. *Adv. Colloid Interface Sci.* **2004**, *110*, 75−95.

(25) Tyrode, E.; Rutland, M. W.; Bain, C. D. Adsorption of CTAB on Hydrophilic Silica Studied by Linear and Nonlinear Optical Spectroscopy. *J. Am. Chem. Soc.* **2008**, *130*, 17434−17445.

(26) Fragneto, G.; Thomas, R. K.; Rennie, A. R.; Penfold, J. Neutron Reflection from Hexadecyltrimethylammonium Bromide Adsorbed on Smooth and Rough Silicon Surfaces. *Langmuir* **1996**, *12*, 6036−6043.

(27) Li, N.; Thomas, R. K.; Rennie, A. R. Neutron Reflectometry of Anionic Surfactants on Sapphire: A Strong Maximum in the

DOI: 10.1021/acs.jpcc.7b09466
J. Phys. Chem. C XXXX, XXX, XXX−XXX

Adsorption near the Critical Micelle Concentration. *J. Colloid Interface Sci.* **2016**, *471*, 81−88.
(28) Li, N. N.; Thomas, R. K.; Rennie, A. R. Effect of pH, Surface Charge and Counter-Ions on the Adsorption of Sodium Dodecyl Sulfate to the Sapphire/Solution Interface. *J. Colloid Interface Sci.* **2012**, *378*, 152−158.
(29) Bharti, B.; Meissner, J.; Gasser, U.; Findenegg, G. H. Surfactant Adsorption and Aggregate Structure at Silica Nanoparticles: Effects of Particle Size and Surface Modification. *Soft Matter* **2012**, *8*, 6573−6581.
(30) Warr, G. G. Surfactant Adsorbed Layer Structure at Solid/Solution Interfaces: Impact and Implications of AFM Imaging Studies. *Curr. Opin. Colloid Interface Sci.* **2000**, *5*, 88−94.
(31) Song, S.-H.; Koelsch, P.; Weidner, T.; Wagner, M. S.; Castner, D. G. Sodium Dodecyl Sulfate Adsorption Onto Positively Charged Surfaces: Monolayer Formation with Opposing Headgroup Orientations. *Langmuir* **2013**, *29*, 12710−12719.
(32) Manne, S.; Cleveland, J. P.; Gaub, H. E.; Stucky, G. D.; Hansma, P. K. Direct Visualization of Surfactant Hemimicelles by Force Microscopy of the Electrical Double Layer. *Langmuir* **1994**, *10*, 4409−4413.
(33) Tiberg, F.; Brinck, J.; Grant, L. Adsorption and Surface-Induced Self-assembly of Surfactants at the Solid-Aqueous Interface. *Curr. Opin. Colloid Interface Sci.* **1999**, *4*, 411−419.
(34) Wanless, E. J.; Ducker, W. A. Organization of Sodium Dodecyl Sulfate at the Graphite-Solution Interface. *J. Phys. Chem.* **1996**, *100*, 3207−3214.
(35) Srinivas, G.; Nielsen, S. O.; Moore, P. B.; Klein, M. L. Molecular Dynamics Simulations of Surfactant Self-Organization at a Solid-Liquid Interface. *J. Am. Chem. Soc.* **2006**, *128*, 848−853.
(36) Tummala, N. R.; Shi, L.; Striolo, A. Molecular Dynamics Simulations of Surfactants at the Silica-Water Interface: Anionic vs Nonionic Headgroups. *J. Colloid Interface Sci.* **2011**, *362*, 135−143.
(37) Liu, Z.; Yu, J.-G.; O'Rear, E. A.; Striolo, A. Aqueous Dual-Tailed Surfactants Simulated on the Alumina Surface. *J. Phys. Chem. B* **2014**, *118*, 9695−9707.
(38) Tummala, N. R.; Liu, S.; Argyris, D.; Striolo, A. Interfacial Water Properties in the Presence of Surfactants. *Langmuir* **2015**, *31*, 2084−2094.
(39) Núñez-Rojas, E.; Domínguez, H. Computational Studies on the Behavior of Sodium Dodecyl Sulfate (SDS) at TiO_2 (Rutile)/Water Interfaces. *J. Colloid Interface Sci.* **2011**, *364*, 417−427.
(40) Domínguez, H. Structural Transition of the Sodium Dodecyl Sulfate (SDS) Surfactant Induced by Changes in Surfactant Concentrations. *J. Phys. Chem. B* **2011**, *115*, 12422−12428.
(41) Núñez-Rojas, E.; Domínguez, H. Computational Studies on the Behaviour of Anionic and Nonionic Surfactants at the SiO_2 (Silicon Dioxide)/Water Interface. *Condens. Matter Phys.* **2016**, *19*, 13602−8.
(42) Dominguez, H.; Goicochea, A. G.; Mendoza, N.; Alejandre, J. Computer Simulations of Surfactant Monolayers at Solid Walls. *J. Colloid Interface Sci.* **2006**, *297*, 370−373.
(43) Shah, K.; Chiu, P.; Jain, M.; Fortes, J.; Moudgil, B.; Sinnott, S. Morphology and Mechanical Properties of Surfactant Aggregates at Water-Silica Interfaces: Molecular Dynamics Simulations. *Langmuir* **2005**, *21*, 5337−5342.
(44) Tummala, N. R.; Striolo, A. Role of Counterion Condensation in the Self-Assembly of SDS Surfactants at the Water-Graphite Interface. *J. Phys. Chem. B* **2008**, *112*, 1987−2000.
(45) Tummala, N. R.; Striolo, A. SDS Surfactants on Carbon Nanotubes: Aggregate Morphology. *ACS Nano* **2009**, *3*, 595−602.
(46) Toofan, J.; Watson, P. The Termination of the α-Al_2O_3 (0001) Surface: A LEED Crystallography Determination. *Surf. Sci.* **1998**, *401*, 162−172.
(47) Hass, K. C.; Schneider, W. F.; Curioni, A.; Andreoni, W. The Chemistry of Water on Alumina Surfaces: Reaction Dynamics from First Principles. *Science* **1998**, *282*, 265−268.
(48) Patwardhan, S. V.; Emami, F. S.; Berry, R. J.; Jones, S. E.; Naik, R. R.; Deschaume, O.; Heinz, H.; Perry, C. C. Chemistry of Aqueous Silica Nanoparticle Surfaces and the Mechanism of Selective Peptide Adsorption. *J. Am. Chem. Soc.* **2012**, *134*, 6244−6256.
(49) Sonnefeld, J. Determination of Surface Charge Density Constants for Spherical Silica Particles Using a Linear Transformation. *J. Colloid Interface Sci.* **1996**, *183*, 597−599.
(50) Emami, F. S.; Puddu, V.; Berry, R. J.; Varshney, V.; Patwardhan, S. V.; Perry, C. C.; Heinz, H. Force Field and a Surface Model Database for Silica to Simulate Interfacial Properties in Atomic Resolution. *Chem. Mater.* **2014**, *26*, 2647−2658.
(51) Berendsen, H.; Grigera, J.; Straatsma, T. The Missing Term in Effective Pair Potentials. *J. Phys. Chem.* **1987**, *91*, 6269−6271.
(52) Jorgensen, W. L. *Encyclopedia of Computational Chemistry*; John Wiley & Sons, Ltd, 2002.
(53) Jorgensen, W. L.; Gao, J. Monte Carlo Simulations of the Hydration of Ammonium and Carboxylate Ions. *J. Phys. Chem.* **1986**, *90*, 2174−2182.
(54) Cygan, R. T.; Liang, J.-J.; Kalinichev, A. G. Molecular Models of Hydroxide, Oxyhydroxide, and Clay Phases and the Development of a General Force Field. *J. Phys. Chem. B* **2004**, *108*, 1255−1266.
(55) Jiménez-Ángeles, F.; Firoozabadi, A. Tunable Substrate Wettability by Thin Water Layer. *J. Phys. Chem. C* **2016**, *120*, 24688−24696.
(56) Kirkwood, J. G. Statistical Mechanics of Fluid Mixtures. *J. Chem. Phys.* **1935**, *3*, 300−313.
(57) Torrie, G. M.; Valleau, J. P. Monte Carlo Free Energy Estimates Using Non-Boltzmann Sampling: Application to the Sub-Critical Lennard-Jones Fluid. *Chem. Phys. Lett.* **1974**, *28*, 578−581.
(58) Kumar, S.; Rosenberg, J. M.; Bouzida, D.; Swendsen, R. H.; Kollman, P. A. The Weighted Histogram Analysis Method for Free-Energy Calculations on Biomolecules. I. The Method. *J. Comput. Chem.* **1992**, *13*, 1011−1021.
(59) Manojlovic, J. Ž. The Krafft Temperature of Surfactant Solution. *Therm. Sci.* **2012**, *16*, 631−640.
(60) Hirata, H.; Ohira, A.; Iimura, N. Measurements of the Krafft Point of Surfactant Molecular Complexes: Insights into the Intricacies of Solubilization. *Langmuir* **1996**, *12*, 6044−6052.
(61) Nosé, S. A. Unified Formulation of the Constant Temperature Molecular-Dynamics Methods. *J. Chem. Phys.* **1984**, *81*, 511−519.
(62) Hoover, W. G. Canonical Dynamics: Equilibrium Phase-Space Distributions. *Phys. Rev. A: At., Mol., Opt. Phys.* **1985**, *31*, 1695−1697.
(63) Hess, B.; Kuztner, C.; van der Spoel, D.; Lindahl, E. GROMACS 4: Algorithms for Highly Efficient, Load-Balanced, and Scalable Molecular Simulation. *J. Chem. Theory Comput.* **2008**, *4*, 435−447.
(64) Abraham, M. J.; Murtola, T.; Schulz, R.; Páll, S.; Smith, J. C.; Hess, B.; Lindahl, E. GROMACS: High Performance Molecular Simulations through Multi-Level Parallelism from Laptops to Supercomputers. *SoftwareX* **2015**, *1−2*, 19−25.
(65) Páll, S.; Abraham, M. J.; Kutzner, C.; Hess, B.; Lindahl, E. In *Solving Software Challenges for Exascale: International Conference on Exascale Applications and Software, EASC 2014, Stockholm, Sweden, April 2−3, 2014, Revised Selected Papers*; Markidis, S., Laure, E., Eds.; Springer International Publishing: Cham, 2015; pp 3−27.
(66) Jiménez-Ángeles, F.; Firoozabadi, A. Contact Angle, Liquid Film, Liquid-Liquid and Liquid-Solid Interfaces in Model Oil-Brine-Substrate Systems. *J. Phys. Chem. C* **2016**, *120*, 11910−11917.
(67) Harwell, J. H.; Hoskins, J. C.; Schechter, R. S.; Wade, W. H. Pseudophase Separation Model for Surfactant Adsorption: Isomerically Pure Surfactants. *Langmuir* **1985**, *1*, 251−262.
(68) Cases, J.; Villieras, F. Thermodynamic Model of Ionic and Non-Ionic Surfactants Adsorption-Abstraction on Heterogeneous Surfaces. *Langmuir* **1992**, *8*, 1251−1264.
(69) Li, B.; Ruckenstein, E. Adsorption of Ionic Surfactants on Charged Solid Surfaces from Aqueous Solutions. *Langmuir* **1996**, *12*, 5052−5063.
(70) Argyris, D.; Ho, T.; Cole, D. R.; Striolo, A. Molecular Dynamics Studies of Interfacial Water at the Alumina Surface. *J. Phys. Chem. C* **2011**, *115*, 2038−2046.

DOI: 10.1021/acs.jpcc.7b09466
J. Phys. Chem. C XXXX, XXX, XXX−XXX

(71) Eng, P. J.; Trainor, T. P.; Brown, G. E., Jr.; Waychunas, G. A.; Newville, M.; Sutton, S. R.; Rivers, M. L. Structure of the Hydrated α-Al_2O_3 (0001) Surface. *Science* **2000**, *288*, 1029−1033.
(72) Catalano, J. G. Weak Interfacial Water Ordering on Isostructural Hematite and Corundum (001) Surfaces. *Geochim. Cosmochim. Acta* **2011**, *75*, 2062−2071.
(73) Duplâtre, G.; Ferreira Marques, M. F.; da Graça Miguel, M. Size of Sodium Dodecyl Sulfate Micelles in Aqueous Solutions as Studied by Positron Annihilation Lifetime Spectroscopy. *J. Phys. Chem.* **1996**, *100*, 16608−16612.
(74) Liu, Y. C.; Chen, S. H.; Itri, R. Ion Correlations and Counter-Ion Condensation in Ionic Micellar Solutions. *J. Phys.: Condens. Matter* **1996**, *8*, A169−A187.
(75) Bergstrom, M.; Skov Pedersen, J. Structure of Pure SDS and DTAB Micelles in Brine Determined by Small-Angle Neutron Scattering (SANS). *Phys. Chem. Chem. Phys.* **1999**, *1*, 4437−4446.
(76) Vass, S.; Pedersen, J. S.; Pleštil, J.; Laggner, P.; Rétfalvi, E.; Varga, I.; Gilányi, T. Ambiguity in Determining the Shape of Alkali Alkyl Sulfate Micelles from Small-Angle Scattering Data. *Langmuir* **2008**, *24*, 408−417.
(77) Berr, S. S.; Caponetti, E.; Johnson, J. S.; Jones, R. R. M.; Magid, L. J. Small-Angle Neutron Scattering from Hexadecyltrimethylammonium Bromide Micelles in Aqueous Solutions. *J. Phys. Chem.* **1986**, *90*, 5766−5770.
(78) Berr, S.; Jones, R. R. M.; Johnson, J. S. Effect of Counterion on the Size and Charge of Alkyltrimethylammonium Halide Micelles as a Function of Chain Length and Concentration as Determined by Small-Angle Neutron Scattering. *J. Phys. Chem.* **1992**, *96*, 5611−5614.
(79) Kung, K. H. S.; Hayes, K. F. Fourier Transform Infrared Spectroscopic Study of the Adsorption of Cetyltrimethylammonium Bromide and Cetylpyridinium Chloride on Silica. *Langmuir* **1993**, *9*, 263−267.
(80) Atkin, R.; Craig, V. S. J.; Wanless, E. J.; Biggs, S. Mechanism of Cationic Surfactant Adsorption at the Solid-Aqueous Interface. *Adv. Colloid Interface Sci.* **2003**, *103*, 219−304.
(81) Velegol, S. B.; Fleming, B. D.; Biggs, S.; Wanless, E. J.; Tilton, R. D. Counterion Effects on Hexadecyltrimethylammonium Surfactant Adsorption and Self-Assembly on Silica. *Langmuir* **2000**, *16*, 2548−2556.
(82) Manne, S.; Gaub, H. E. Molecular Organization of Surfactants at Solid-Liquid Interfaces. *Science* **1995**, *270*, 1480−1482.

DOI: 10.1021/acs.jpcc.7b09466
J. Phys. Chem. C XXXX, XXX, XXX−XXX